IMPACTS OF WETTABILITY ON OIL RECOVERY IN FRACTURED CARBONATE RESERVOIRS

Arne Graue, Robert W. Moe and Thomas Bognø
Department of Physics, University of Bergen, Norway

Abstract

Visualization of the effects of various wettability conditions on oil recovery in fractured carbonate reservoirs is demonstrated in two-dimensional in-situ imaging experiments in large blocks of chalk and by numerical simulations. Recovery mechanisms are shown to change with a change in wettability. Iterative comparison between experimental work and numerical simulations has been used to predict oil recovery mechanisms in fractured chalk as a function of wettability. Selective alteration of wettability, by aging in crude oil at elevated temperature, produced chalk blocks which were strongly-water-wet and moderately-water-wet, but with identical pore geometry. Large scale, nuclear-tracer, 2D-imaging experiments monitored waterflooding the blocks of chalk, first whole then fractured. Capillary pressure and relative permeabilities at each given wettability were experimentally measured and used as input for the simulations. Mixing of injection water and in-situ water was determined both for unfractured and fractured reservoirs by labelling the waters with different nuclear tracers.

A simulator for fractured reservoirs has been validated by large scale experiments with 2D in-situ imaging information. Experimentally obtained capillary pressure (Pc) and relative permeability (Kr) -input data to the simulator have been evaluated by history matching in-situ saturation distribution development as well as the production profile. For a low permeability increase after fracturing, for both unfractured and fractured chalk, the amount and rate of oil recovery by waterflooding were similar for strongly-water-wet and moderately-water-wet conditions, but the in-situ saturation distributions are shown to be significantly affected by the wettability conditions. This indicates that the recovery mechanisms change towards more viscous dominant flow regimes at less water-wet conditions.

Introduction

To determine the impacts from wettability on oil recovery mechanisms in fractured reservoirs scaled-up laboratory waterflood imaging experiments with corresponding numerical simulations have been performed. To investigate the simultaneous interaction between capillary forces, viscous forces and gravity and to reduce the impacts from capillary end effects blocks of outcrop rock are used instead of core plugs. Imaging the local in-situ 2D-saturation development of the individual water compositions, the in-situ water and the injection water, the mixing of the waters is determined.

A previous series of laboratory waterflood experiments, using blocks of fractured chalk, where the advancing waterfront was tracked by the nuclear tracer 2D-imaging technique (ref. 1-3,19), has shown that altering the wettability from strongly-water-wet to moderately-water-wet conditions had minor impacts on the amount and the rate of oil production. However, the in-situ saturation development was significantly different, indicating differences in oil recovery mechanisms (ref. 4,18,20). The main objective for the current experiments was to determine the oil recovery mechanisms at different wettability conditions. The term moderately-water-wet in this paper is defined to cover the wettability conditions reflecting an Amott-Harvey water index,

I_w, in the range 0.5 – 0.8. Earlier we reported a technique that reproducibly altered wettability in outcrop chalk by aging the rock material in stock tank crude oil at elevated temperature for a selected period of time (ref. 5). Utilizing this technique we have produced larger blocks of outcrop chalk at selected wettabilities, which were waterflooded, first as a whole block, then again after the blocks were fractured and reassembled. Earlier work reported on experiments using an embedded fracture network, while in this work two interconnected fracture networks, one that introduced hydraulic contact from inlet to outlet and one that also contained an isolated block surrounded by fractures, have been studied. Results on how injection water mixed with in-situ water improved the interpretation of the recovery mechanisms by providing information on the composition of the produced water.

A second objective of these experiments has been to validate a full field numerical simulator for prediction of the oil production and the in-situ saturation dynamics for these waterfloods. In this process quality control of the experimentally measured capillary pressure and relative permeability data, used as input for the simulator, has been performed at strongly-water-wet and moderately-water-wet conditions. Optimization of either Pc-data or kr-curves for the chalk matrix in the numerical simulations of the whole blocks at different wettabilities gave indications of which of these input data could be most trusted. History matching both the production profile and the in-situ saturation distribution development gave higher confidence in the simulations of the fractured blocks, where only the fracture representation was a variable.

Experimental

Rock and fluids: Four chalk blocks, CHP-8, CHP-9, CHP-12 and CHP-14, approximately 20 cm × 10 cm × 5 cm thick, were cut from large pieces of Rørdal outcrop chalk obtained from the Portland quarry near Ålborg, Denmark. Before the blocks were epoxy coated, local air permeability was measured at each intersection of a 1 cm by 1 cm grid on both sides of the blocks using a minipermeameter. The permeability maps indicated homogeneous blocks on a cm scale. The blocks were vacuum evacuated and saturated with brine containing 5wt% NaCl + 3.8wt% $CaCl_2$. Fluid data is found in Table 1. Porosity was determined from weight measurements and the permeability was measured across the epoxy coated blocks (see Table 2).

Initial Sw: Immobile water saturations of 22-28%PV were established for all blocks by oilflooding with a maximum differential pressure of 125 kPa/cm. In order to obtain a uniform, low initial water saturation, S_{wi}, oil was injected alternately, at both ends. To add experience to the earlier work emphasizing oil recovery in fractured chalk (ref. 4-12,15-18) studying waterfloods of whole blocks and fractured blocks with embedded fracture networks, the following experimental schedule was outlined: The strongly-water-wet block CHP-9 was waterflooded with an interconnected fracture network as shown in Figure 1c. The strongly-water-wet block CHP-12, was waterflooded first as a whole block then again after it had been oilflooded back to Swi, and then fractured and reassembled into the desired interconnected fracture network shown in Figure 1d. This experimental procedure was then repeated on the two blocks aged to moderately-water-wet conditions, CHP-8 and CHP-14. Block CHP-8 was waterflooded first as a whole block then with an embedded fracture network shown in Figure 1b and finally with an interconnected fracture network as shown in Figure 1c. CHP-14 was waterflooded as a whole block and then with the interconnected fracture network as shown in Figure 1d.

Oil flooding and aging: The strongly-water-wet blocks were oilflooded using decane. Oilfloods of the moderately-water-wet blocks used stock tank crude oil from a chalk reservoir in the North Sea and were carried out at 90°C in a heated pressure vessel. The pressure vessel was capable of holding up to 1000 kPa of confining pressure so that a maximum pressure drop of 900 kPa could be applied across the block. This resulted in a lower limit for the Swi to be 25%PV. Because of possible wax problems with the North Sea crude oil used for aging, the temperature was maintained at 90° C as long as crude oil was in the block. After aging was completed, the crude oil was flushed out with decahydronaphthalene (decalin) which in turn was flushed out by n-decane at 90° C. Decalin was used as buffer between the decane and the crude oil to avoid asphaltene precipitation. Decane and brine were used during the waterfloods for all blocks.

Wettability testing: To get an initial indication of the wettability of the blocks aged in crude oil at 90°C to obtain moderately-water-wet conditions, duplicate plug samples drilled from the same chunk of chalk that the block was taken from, received the same treatment as the blocks. A measure of the wettability was then obtained by the Amott-Harvey test (ref. 13). After the waterfloods were terminated core plugs were drilled out of each of the blocks and wettability measurements were conducted on the plugs. The aging process produced chalk blocks CHP-8 and CHP-14 at moderately-water-wet conditions, reflecting an Amott index to water, Iw, of 0.8 and 0.6, respectively. Thus we established three physical reservoir models with similar mineralogy and pore geometry but with different wettabilities.

Fractures: The fractures were created, when the whole block had been driven back to S_{wi} after the first waterflood, by cutting the block with a band saw. When reassembling the blocks, tape was placed over the fractures to prevent the epoxy, used to reseal the core, from entering the fractures. A 2 mm strip of Teflon was placed at the outer, lower, edge of the open fracture to assure a well defined open volume. A pressure of 10 kPa across the fractures was applied to mechanically hold the different parts of the block in position while the epoxy cured. The different fracture orientations and arrangements of the individual pieces for the reassembled blocks, are shown in Figure 1b-d. The xy coordinates are used to identify location. The individual blocks are identified as Block A1 and A2, the inlet blocks, Block B1 and B2, the central blocks which were surrounded by fractures and Block C1 and C2, the outlet blocks. Both an open fracture, no possible capillary contact, and several "closed" fractures, with contact between the adjacent matrix blocks, were formed. The "closed" fractures were intended to provide at least some capillary continuity of both fluid phases across the fracture. The open vertical fracture at 13 cm was created by sliding Block B1 and B2 to the left as far as possible producing an open fracture with the width of one saw cut, ca. 2 mm. The other fractures were "closed", i.e. the pieces were placed butt to butt when reassembling the block, with an axial force applied during the reassemble. After reassemble, the fracture network was filled with decane using a syringe. This fracture network assured hydraulic contact from the inlet to outlet end; i.e. from “injector” to “producer”. The blocks were positioned vertically during flooding, thus gravity was aligned with the vertical fractures.

Saturation monitoring: Nuclear-tracer, 2D-imaging experiments monitored waterflooding of the chalk blocks, first whole, then fractured. 2-D brine saturations were determined by measuring gamma ray emission from ^{22}Na and ^{60}Co separately dissolved in brines used alternately as injection water and in-situ water. The blocks were mounted in a vertical position while flooded and a saturation map was produced at each specified point in time, according to the grid shown in

Figure 1. Each individual saturation map is identified by a scan number, cfr. e.g. Figure 2. Each scan number is preceded by a letter and number to identify each block, e.g. P12 and P14 for CHP-12 and CHP-14, respectively. The oil and waterfloods were labeled O and W, respectively, with the first digit being the flood number and the two digits following the dash indicating the chronological sequence of scans. Thus P12W2-09 is the 9th scan of the 2nd water flood on block CHP-12.

The working principle of the nuclear tracer technique has been described in detail (ref.1-4, 19). The outline of the experimental sequence used to flood the unfractured and fractured blocks, while using 2-D imaging to determine the distribution of brine saturation, and the results are summarized in Table 2.

The two tracers used for labeling the connate and injected water, are not ideal since both tracers are soluble in both fluids. However, the objective of this work is to look for development of a bank of the initial brine ahead of the connate brine. Mixing by diffusion and dispersion will be exaggerated due to the tracers being soluble in both of the brines. However, due to relatively short experiment duration it turned out that movement of the individual compositions could be readily identified.

Results and Discussion

Strongly-water-wet blocks

Waterfloods of whole blocks, both at strongly-water-wet and moderately-water-wet conditions have been shown to be similar with respect to oil production and in-situ saturation development (ref. 4). Figure 2 and Figure 3 show how the water displaces the oil in a typical whole block waterflood. During all of the waterflood experiments the brine was injected from the left side of the image and the displaced fluids exited at the right side of the image. Figure 2 shows the dynamic saturation development for the injection water displacing the oil from the whole block CHP-12, Scans P12W1-00 to Scan P12W1-32. The corresponding dynamics for the in-situ water is shown in Fig.3. Uniform initial water saturation was measured for CHP-12 as the first saturation map, P12W1-00 in Figure 3. A dispersed waterfront flushed out 43%PV of decane. Increasing the flow rate has been shown to produce a less dispersed waterfront, ref. 1. In waterfloods starting at higher initial water saturation there was essentially no waterfront at all, i.e. a uniform increase in water saturation was recorded, ref. 10. A uniform final water saturation was obtained at ca. Sw=68%PV. Figure 4 shows the development of the in-situ and total water saturations averaged across the block perpendicular to the flow direction in a 1-D saturation plot. As we have experienced earlier for core floods, the in-situ water banked up in front of the injection water, but compared to the earlier work, the banking was less pronounced and more dispersed, probably due to the lower flow rates applied in these block experiments. All of the in-situ water was displaced during the waterflood.

When the blocks were driven back to S_{wi} an excellent reproduction of the original water saturation and saturation distribution was generally obtained, see Table 2. Good agreement was obtained between the nuclear tracer determined in-situ saturation and mass balance.

The blocks were then cut with a band saw into the six shapes shown in Figure 1. The nuclear tracer saturation measurements of the whole and the assembled fractured block indicated that the cutting process did not measurably alter the saturation distribution at S_{wi}, as was also observed in previous experiments (ref. 4,10,11).

The left side of Figure 5 shows the experimental results of the time development of the total water saturation while waterflooding the fractured, strongly-water-wet block CHP-12. An interconnected fracture network that isolated blocks B1 and B2 was used,(see Figure 1d). The brine saturation increased as a dispersed front through Block A2, the continuous inlet block,

Scans P12W2-00 to P12W2-08. In Scan P12W2-08 Block B1 and B2 were still at, or close to, S_{wi} while the matrix just across the fracture in Block A1 and A2 was approaching S_{wf}. This suggested a limited rate of transport of fluids across the "closed" vertical fracture at 4 cm and the horizontal fracture at 5.0 cm. In fact the brine did not appear to cross any of the fractures before the saturations in all of Block A1 and A2 were close to their final water saturation. After Block A1 and A2 reached high brine saturations and the fractures were filled with brine, the brine entered Block B1 and B2, Scan P12W2-12. The general appearance of Block B1 and B2 in Scan P12W2-12 suggest that the brine entered gradually from both the horizontal and vertical fracture between Block A1 and A2 and Block B1 and B2. However, little, if any, water had gone across the fracture at 13 cm into Block C at the time when Scan P12W1-12 was taken. When Blocks B1 and B2 approached their final water saturation, water movement into Block C1 and C2, the outlet blocks, was recorded (see scan P12W2-17). Higher water saturation in the mid- to upper part of Block C2 at the outlet-end, shown in scan P12W2-17, indicated that the wetting phase crossed the "closed" fracture before any significant amount of water accumulated, by gravity segregation, in the bottom of the open fracture. The latter was observed in some earlier experiments performed at strongly-water-wet conditions (ref. 4,10,11).

The in-situ water saturation dynamics for this waterflood, shown in Figure 6, showed that the in-situ water was gradually displaced, but no banking was recorded. Even after 1.0 PV of water had been injected 10%PV of in-situ water remained at the inlet end of the block and near 30%PV of the in-situ brine remained at the outlet. This indicated that after fracturing, which increased the endpoint effective permeability to water at Sor by a factor of 220, less injection water was flushed through the matrices thus causing the displacement of in-situ water to be less efficient.

It has earlier been shown that there is essentially no difference in total oil recovery for a strongly water-wet block between waterfloods on the whole block and a fractured block with embedded fractures (ref. 4,10,11). In Figure 7 the oil production for the fractured block CHP-12, with interconnected fractures, is compared to earlier results on strongly-water-wet whole blocks and blocks with embedded fractures. From the figure it is evident that water breakthrough in the block with interconnected fractures occurred somewhat earlier and the block produced slightly less oil. The hydraulic contact from inlet to outlet also resulted in a short period with two-phase production, giving less sharp water cut. This trend is more noticeable for the higher permeability increase with connected fractures, but the reduction in oil recovery is still minor. A total of 42%PV oil was produced. We interpret this as a result of the recovery mechanisms being controlled by spontaneous imbibition and thus the endpoint saturation is predominantly determined by the capillary forces.

Moderately-water-wet blocks

Block CHP-8 was treated to provide moderately-water-wet conditions, although it turned out to be more water-wet than expected. Figure 8a shows the imbibition characteristics for the twin plugs treated similarly to the block and for the three plugs drilled from the block. Imbibition characteristics for one strongly water-wet plug and two plugs at nearly-neutral-wet conditions are included in Fig.8a for comparison. Compared to the strongly-water-wet baseline a consistent change in wettability towards less water-wet conditions, longer induction time, lower imbibition rate and lower final water saturation were obtained. However, the twin plugs both exhibit an Amott index to water of 0.5, while all three drilled out plugs consistently had Iw=0.8.The aging technique used for CHP-8, was therefore modified when CHP-14 was aged. Crude oil was continuously flushed through the block CHP-14 during aging. Figure 8b shows the imbibition characteristics for the twin plugs aged in this manner and for the drilled out plugs from CHP-14.

The inlet end of the block gave a wettability index to water of Iw=0.4. The central part exhibited more water-wet conditions, corresponding to a wettability index to water of Iw=0.7, while the outlet end showed Iw=0.8. The experience gained from using dynamic aging resulted in a new practice of reversing the flow direction several times during aging.

Results on waterflooding CHP-8 can be found in ref. 18. The main conclusion from waterflooding this block first, as a whole block, second with embedded fractures and third, with interconnected fractures, was that even at a wettability of Iw=0.8 the in-situ saturation development for the waterfloods of the fractured block showed the same behavior previously seen for the less-water-wet conditions (ref. 4,18). This implied that the wetting phase crossed the fractures early and no significant capillary hold-up at the fracture, as for strongly-water-wet conditions, were recorded (ref. 4,11,18).

The moderately-water-wet block CHP-14 was waterflooded first as a whole block, and then with an interconnected fracture network. For the whole block waterflood a dispersed water front swept out 43%PV of oil from the block. As for the waterflood of the strongly-water-wet whole block CHP-12, significant banking of the in-situ water was observed and all of the in-situ water was displaced for the whole block waterflood of CHP-14.

Figure 9 shows the time development of the injected brine saturation during the waterflood of the moderately-water-wet fractured block, CHP-14, with the interconnected fracture network shown in Figure 1d. The brine saturation increased as a dispersed front through Block A1, the upper continuous inlet block, and into Block B1 and B2, (Scans P14W2-00 to P14W2-10). In contrast to earlier experiments of waterflooding moderately-water-wet fractured blocks, the fractures had significant effect; transport of fluids along the fractures was observed and water accumulated in the bottom of the open fracture at 13cm. This was probably due to a higher permeability increase after fracturing, compared with earlier experiments at moderately-water-wet conditions. The permeability to water at Sor increased by a factor of 11 relative to the whole block. However, some capillary contact across the "closed" fractures had apparently been established, as had been the case in earlier experiments. Gravity segregation in the open vertical fracture was observed. The water entered Block C2 from the bottom of the open fracture and across the "closed" vertical fracture at 13 cm.

The dynamic behavior of the in-situ water is shown in Figure 10. The in-situ water was gradually displaced, but no banking was recorded. Even after 1.0 PV of water had been injected, more than 10%PV of in-situ water remained, particularly in the isolated blocks B1 and B2. This indicated that after fracturing, less injection water was flushed through the matrices, thus causing the displacement of in-situ water to be less efficient.

Oil production from waterfloods on the whole and fractured moderately-water-wet block CHP-14 is shown in Figure 7. For the whole block, at moderately-water-wet conditions, oil recovery was similar to the strongly-water-wet case. When fractured, the block showed earlier water breakthrough and a longer transition zone with two-phase production. Less oil, 32%PV, was produced.

This behavior, that total oil recovery from each block was reduced by a consistent, but small amount, after fracturing the blocks as long as the permeability increase was low, is consistent with results for all the different wettability conditions reported in ref. 4. At strongly-water-wet conditions, a permeability increase after fracturing of about 50 did not reduce the oil production compared to the baseline whole block experiment, as recorded for block CHP-9. Even a permeability increase of about 200, as for block CHP-12, did not reduce the oil production by any significant amount, for the fractured strongly-water-wet blocks. At moderately water-wet conditions, however, the reduction in oil production was about 10%PV, when the effective water permeability at Sor increased after fracturing by a factor of about 10.

The pattern of water movement during the first waterflood of the strongly-water-wet, fractured block CHP-12, indicated that there was little capillary contact, for the water phase, between Blocks A2 and C1 and C2 across the upper portion of the fracture at 13 cm. If there had been significant capillary continuity, water would have readily crossed the fracture and saturated the upper portion of Block C1 and C2 during the early stages of invasion of Block A. However, gravity segregation of the fluids in the fractures indicated fairly open fractures at 13 cm for CHP-12. For the less water-wet block, CHP-14, the water entered Block C1 and C2 both from the bottom of the open fracture and from the "closed" vertical fracture at 13 cm. This indicated a combined effect resulting from the fracture enhanced permeability and reduced influence of the "closed" fractures on the flow pattern during waterflood when the wettability changed towards moderately-water-wet. It seems unlikely that this was due to better capillary contacts between the blocks in CHP-14, since the reassembling procedure was similar for all the blocks, and this effect has been consistently observed in earlier experiments. We speculate that a) capillary holdup of the wetting phase at less water wet conditions is reduced or b) that water droplets are being formed at the exit end of the block and establish wetting phase bridges across the fractures when the contact angle increases as wettability is changed to less water-wet conditions. The latter displacement mechanism depends on the fracture aperture, the viscous pressure in the wetting phase, i.e. the applied differential pressure and the wettability conditions. We believe one of these two mechanisms or a combination of the two are responsible for the reduced impact of the fractures on the water flood at less water-wet conditions.

Capillary pressure and relative permeability have been measured in chalk core plugs at strongly-water-wet, moderately-water-wet and nearly-neutral-wet conditions, ref. 17. Plug wettability was selectively altered by aging outcrop chalk plugs, at Swi, in crude oil at an elevated temperature for selected periods of time. This procedure reproducibly produced the desired wettability while keeping the pore network structure and the mineralogy constant. Aging to a less-water-wet state, significantly reduced spontaneous brine imbibition rate and endpoint. However, it did not reduce the total movable oil, i.e. imbibition plus forced displacement. In fact, the total movable oil generally increased slightly with reduced water wettability, however, at the cost of higher differential pressures. Reduced water wettability also lowered the drainage threshold pressure. Reproducibility of repeat imbibition tests on individual plugs indicated that the wettability alteration was permanent. These experiments were conducted in order to obtain input data for capillary pressure and relative permeability at a range of wettability conditions for numerical simulations. A full field simulator for fractured reservoirs, SENSOR (ref. 14), was used to simulate numerically oil recovery from the fractured blocks. First, the simulations were run using experimental values for both capillary pressure and relative permeabilities at the different wettabilities. Then, to improve the history matching for both the oil production and the dynamics of the in-situ saturation development, the input data was adjusted. Capillary pressure curves were optimized while keeping the experimentally derived relative permeabilities constant and then the relative permeabilities were optimized with the experimental capillary pressure curves held constant. This procedure gave an indication of the validity of the measured values. The overall best match with the experiments for all the simulations was always obtained using the experimentally obtained capillary pressure curves and optimized relative permeabilities.

Figure 11 shows the resulting history match for waterflooding the whole block CHP-12. Figure 12 shows the corresponding match of the oil production. In the right side of Figure 5 the simulation of the waterflood of the fractured block CHP-12 is shown. A satisfactory history match was obtained. Figure 13 shows the match of the oil production for the moderately-water-wet block CHP-14, when waterflooded as a whole block. In this simulation the experimental capillary pressure curves and the optimized relative permeability curves were used. However, the

history match was not good, probably due to the heterogeneous wettability conditions in this block. A new simulation was therefore run with three sets of capillary pressure and relative permeability curves, reflecting the variation in wettability recorded in the drilled out plugs. The revised simulation is shown in Figure 14.

To obtain a good history match, the degree of capillary contact used in the simulations had to be increased for the less-water-wet cases. Since the wettability information should be in the capillary pressure and relative permeability data we interpret this as an indication that an additional mechanism, not taken into account in the model, causes the wetting phase to cross the fractures at less-water-wet conditions. High spatial resolution experiments using NMR tomography imaging is underway to test this interpretation by study of the fluid flow inside the fractures.

Conclusions

From two-dimensional in-situ saturation development during waterfloods at strongly-water-wet and at moderately-water-wet conditions in large fractured blocks of chalk the following conclusions can be drawn:

- Water movement during water flooding was significantly affected by the presence of fractures at strongly water-wet conditions, but not at moderately-water-wet conditions.
- For unfractured and fractured chalk the oil recovery by waterflooding was similar for strongly-water-wet chalk and moderately-water-wet chalk, when the permeability increase after fracturing was low.
- Production rate and total oil production was not affected by fractures at strongly-water-wet conditions, but for moderately-water-wet chalk oil recovery was reduced when the permeability increase after fracturing was high.
- Open fractures act as barriers to flow at strongly-water-wet and moderately-water-wet conditions.
- Experimentally obtained Pc and kr input data have been evaluated by history matching in-situ saturation distribution development as well as the production profile. The overall best match between the simulations and the experiments was obtained using the experimentally obtained capillary pressure curves and optimizing the relative permeabilities.
- A simulator for fractured reservoirs was validated by large scale experiments with 2D-in-situ imaging information.
- Including wettability heterogeneities in the numerical simulation of the waterfloods improved the history match.

Nomenclature

D= diameter [cm]
I= Amott wettability index
k= permeability [md]
L= length [cm]
p= paper
P= Pressure [bar]
R= oil recovery [%]
S= saturation
t= time [days]
T= temperature [°C]

Greek

μ= viscosity [cp]
ρ= density [g/cm^3]
σ= interfacial tension, [IFT]
ϕ= porosity[%]

Subscripts

a= aged
C= capillary
d= displacement
eff= effective
f= final
i= initial
im= imbibition
o= oil
si= spontaneous imbibition
w= Amott wettability index
k= permeability [mD]
S= saturation
f= final
i= initial
w=water

References

1. Lien, J.R., Graue, A. and Kolltveit, K.: “A Nuclear Imaging Technique for Studying Multiphase Flow in a Porous Medium at Oil Reservoir Conditions”, Nucl. Instr. & Meth., A271, 1988.
2. Graue, A., Kolltveit, K., Lien, J.R. and Skauge, A.: “Imaging Fluid Saturation Development in Long Coreflood Displacements”, SPEFE, Vol.5, No.4, 406-412, (Dec., 1990).
3. Graue, A.: "Imaging the Effect of Capillary Heterogeneites on Local Saturation Development in Long-Core Floods", SPEDC, Vol. 9, No. 1, March 1994.
4. Graue, A., Viksund, B.G., Baldwin, B.A., Spinler, E.: "Large Scale Imaging of Impacts of Wettability on Oil Recovery in Fractured Chalk", SPE Journal, Vol 4, No. 1, March 1999.
5. Graue, A., Viksund, B.G., Baldwin, B.A: “Reproducible Wettability Alteration of Low-Permeable Outcrop Chalk”, SPE Res. Eng. and Eval., April, 1999.
6. Graue, A. and Viksund, B.G.: “Imaging Immiscible Two Phase Flow in Low Permeability Chalk – Emphasis on Recovery Mechanisms and Scaling”, Ext.Abs.Proc.: EAPG/AAPG Special Conference on Chalk, Copenhagen, Denmark, (Sept. 7-9, 1994).
7. Graue, A.: “Nuclear Tracer Saturation Imaging of Fluid Displacement in Low-Permeability Chalk”, SPE 25899, Proc.: SPE Rocky Mountain Regional/Low Permeability Reservoirs Symposium, Denver, CO, USA, (April 26-28, 1993).
8. Viksund, B.G., Hetland, S., Graue, A. and Baldwin, B.A.: "Imaging Saturation during Flow in Fractured Chalk: Emphasizing Recovery Mechanisms, Capillary Continuity and Scaling", Reviewed Proc.: 1996 Int. Symp. of the Society of Core Analysts, Montpellier, France, (Sept. 8-10, 1996).
9. Torsaeter, O.: “An Experimental Study of Water Imbibition in Chalk from the Ekofisk Field”, SPE 12688, Proc.: SPE/DOE Fourth Symposium on EOR, Tulsa, OK, (April 1984).
10. Viksund, B.G., Graue, A., Baldwin, B. And Spinler, E.: “2-D Imaging of waterflooding a Fractured th Chalk Research Symposium, Reims, France, (Oct. 7-9, 1996).
11. Viksund, B.G., Eilertsen T., Graue, A., Baldwin, B. and Spinler, E.: "2D-Imaging of the Effects from Fractures on Oil Recovery in Larger Blocks of Chalk", Reviewed Proc.: International Symposium of the Society of Core Analysts, Calgary, Canada. (Sept. 8-10, 1997).
12. Graue, A., Tonheim, E. and Baldwin, B.: “Control and Alteration of Wettability in Low-Permeability Chalk”, Proc.: 3rd International Symposium on Evaluation of Reservoir Wettability and Its Effect on Oil Recovery, Laramie, Wy., USA, Sept., 1995.
13. Amott. E.: "Observations Relating to the Wettability of Porous Rock", Trans., AIME 1959 216, 156-162.
14. Coats, K.H., Thomas, L.K., and Pierson, R.G.: “Compositional and Black Oil Reservoir Simulation”, SPE29111, 13th SPE Reservoir Simulation Symposium, San Antonio, Texas, Febr. 1995.
15. Viksund, B.G., Morrow, N.R., Ma, G., Wang, W., Graue, A.: «Initial Water Saturation and Oil Recovery from Chalk and Sandstone by Spontaneous Imbibition», reviewed proc.: 1998 International Symposium of Core Analysts, The Hague, Sept., 1998.
16. Spinler, E.A, Baldwin B. A., Graue, A.: ”Simultaneous Measurement of Multiple Capillary Pressure Curves from Wettability and Rock Property Variations Within Single Rock Plugs”, SCA9957, Reviewed Proc.: 1999 International Symposium of Core Analysts, Golden, Co., USA, Aug. 1-4, 1999.
17. Graue, A., Bognø, T., Moe, R.W., Baldwin, B.A., Spinler, E.A., Maloney, D., Tobola, D.P.: ”Impacts of Wettability on Capillary Pressure and Relative Permeability”, SCA9907, Reviewed Proc.: 1999 International Symposium of Core Analysts, Golden, Co., USA, Aug. 1-4, 1999.
18. Graue, A., Bogno, T.: “Wettability Effects on Oil Recovery Mechanisms in Fractured Reservoirs”, SPE56672, 1999 SPE Annual Tech. Conf. And Exh., Houston, TX, Oct. 3-6, 1999.
19. Bailey, N.A., Rowland, P.R., Robinson, D.P.: “Nuclear Measurements of Fluid Saturation in EOR Flood Experiments”, Proc.: 1981 European Symposium on Enhanced Oil Recovery, Bornmouth, England, Sept. 21-23, 1981.
20. Graue, A., Mow, R.W., Baldwin, B.A.: “Comparison of Numerical Simulatons and Laboratory Waterfloods with In-Situ Saturation Imaging of Fractured Blocks of Reservoir Rocks at Different Wettabilities”, SPE59039, 2000 SPE Internatl. Petr. Conf. And Exh., Villahermosa, Mexico, Febr. 1-3, 2000.

Table 1. Fluid Properties				
Fluid	Density ^{3}]	Viscosity ^{o}C	Viscosity ^{o}C	Composition
Brine	1,05	1,09		5 wt% NaCl + 3.8 wt% $CaCl_2$
n-Decane	0,73	0,92		
Decahydronaphtalene	0,896			
Crude oil	0,849	14,3	2,7	

Table 2. Experimental Data for Chalk Blocks									
Block	CHP-8			CHP-9		CHP-12		CHP-14	
Outcrop	Portland			Portland		Portland		Portland	
Location	Ålborg			Ålborg		Ålborg		Ålborg	
Length (cm)	19,9			19,8		20,0		20	
Height (cm)	10,0			10,0		10,0		10,0	
Thickness (cm)	5,5			5,4		5,0		5	
Abs. Permeability (mD)	2,3			3,8		2,3		2,2	
Porosity (%)	47,6			48,1		45,7		46,2	
Pore Volume (ml)	516			514		457		450	
MISC. FLOOD # :	1			1		1		1	
Flow Rate (ml/hr)	10			40		15		20	
OILFLOOD # :	1	2	3	1		1	2	1	2
Oil Viscosity (cP)	2,7	0,92	0,92	0,92		0,92	0,92	2,7	0,92
Swi (%PV)	100	76	72	100		100	67	100	71
dSw (%PV)	72	43	37	73		76	44	72	49
Swf (%PV)	28	33	35	27		24	23	28	22
Max Pressure (Bar)	10	24	24	24		25	25	9,5	25
Endpoint Eff. Perm. to oil (mD)	3	1,3[a]/1,3[b]	1,0[b]/42[c]	3,3[a]/156[c]		2,5	2,4[a]	0,4	2,4[a]
AGING :	YES			NO		NO		YES	
Aging Temp. (deg. C)	90							90	
Aging Time (days)	83							1,6	
Amott index after aging	0,53			1		1		0,6	
Oil flooding prior to imb. :									
Decaline (PV)	5							5	
n-Decane (PV)	5							5	
Endpoint eff. Perm. to oil (mD)	2,4							0,4	
WATERFLOOD # :	1	2	3	1	2	1	2	1	2
Block Condition	Whole	Fractured	Fractured	Fractured	Fractured	Whole	Fractured	Whole	Fractured
Cutting		Band Saw	Band Saw	Band Saw	Band Saw		Band Saw		Band Saw
Oil Viscosity (cP)	0,92	0,92	0,92	0,92	0,92	0,92	0,92	0,92	0,92
Swi (%PV)	28	33	35	27	67	24	23	28	22
dSw (%PV)	45	39	40	40	1	44	42	43	32
Swf (%PV)	73	72	75	67	68	67	65	71	54
Endpoint Eff. Perm. to water (mD)	0,4	0	15	87[c]	42	0,7	155	0,2	2,2
Oil Recovery (%OIP)	63	58	62	55	3	57	55	59	41
Flow Rate (ml/hr)	1	1	1	1	20	1	1	1	1

[a)] Whole block

[b)] Fractured block, embedded fracture network

[c)] Fractured block, interconnected fracture network

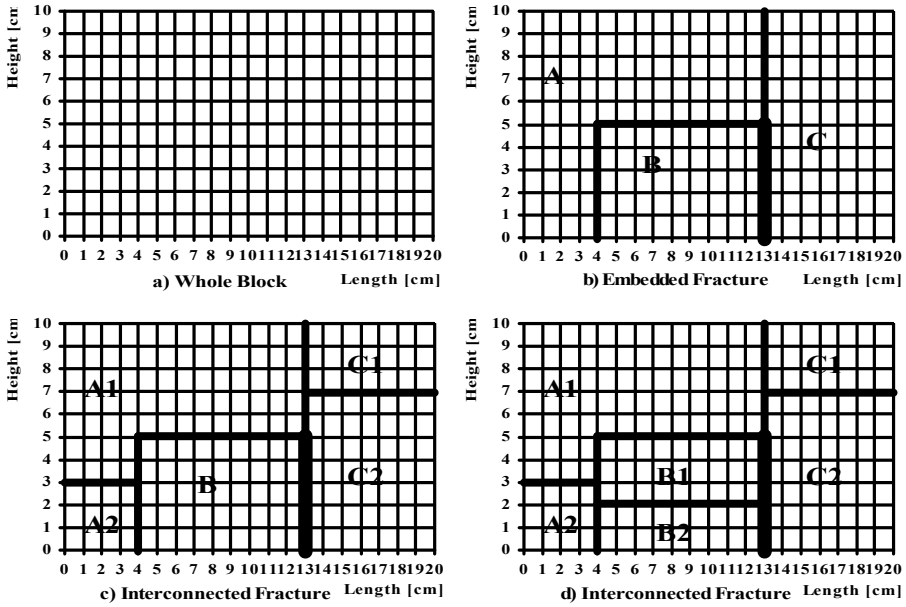

Fig.1 The fracture networks used in the experiments and the simulations.

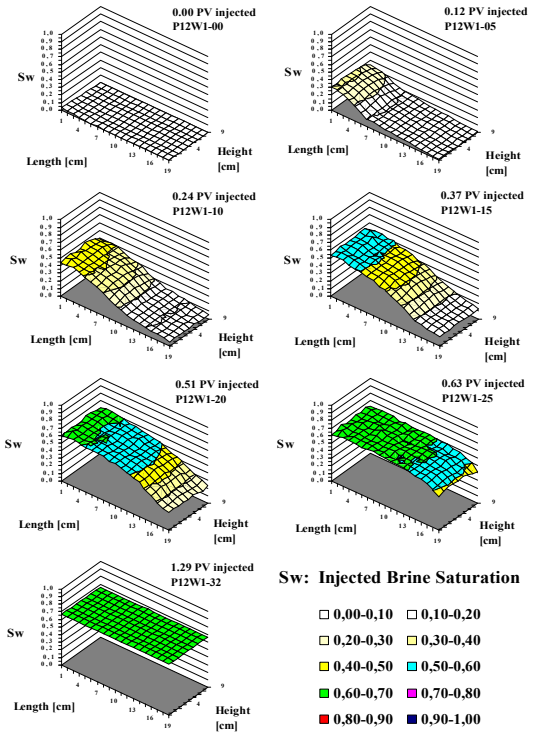

Fig.2 Saturation development of the injected water while waterflooding whole block CHP-12.

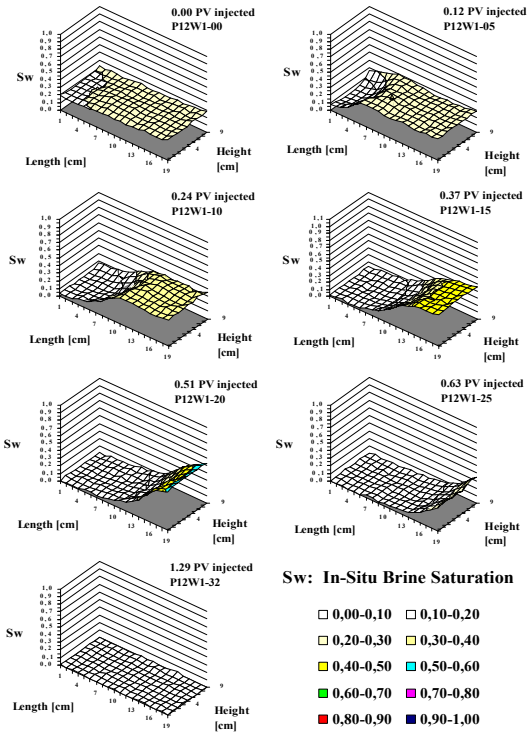

Fig.3 Saturation development of the in-situ water while waterflooding whole block CHP-12.

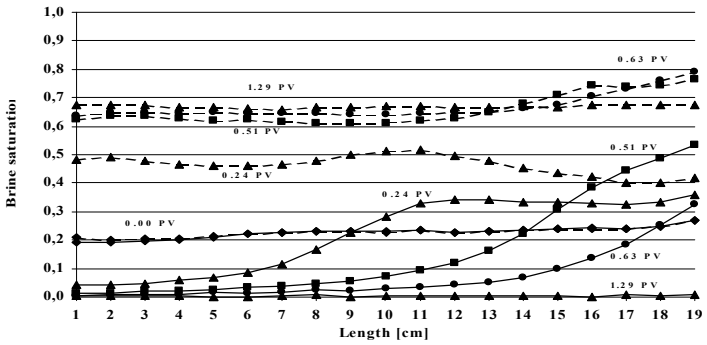

Fig.4 1D saturation profiles of the total water (dashed line) and the in-situ water (solid line) of the whole block CHP-12.

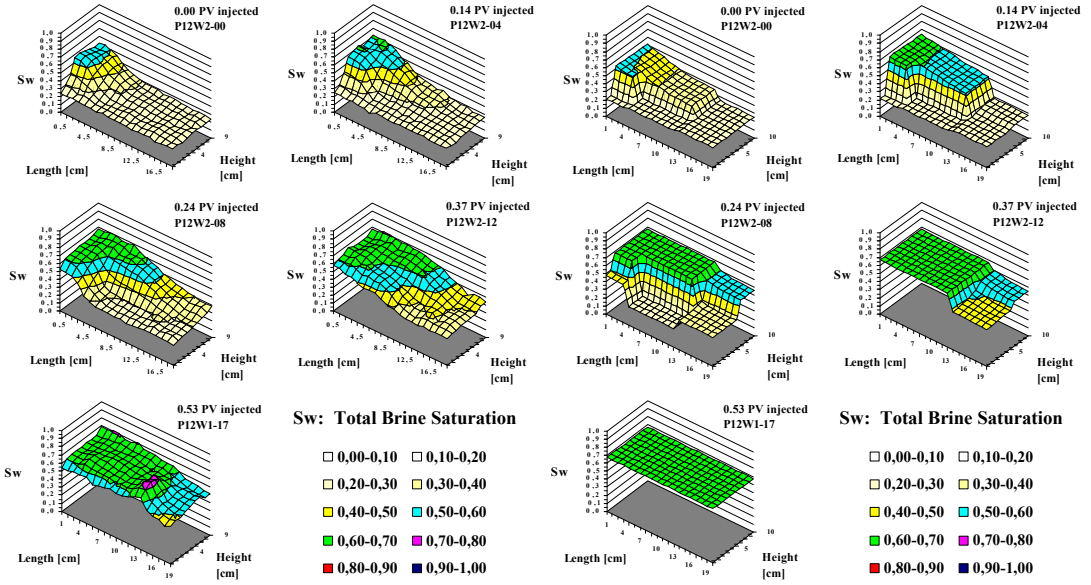

Fig.5 Comparison of experimental, left two columns, and simulated, rightmost two columns, in-situ saturation development for the second waterflood of the strongly water-wet block CHP-12.

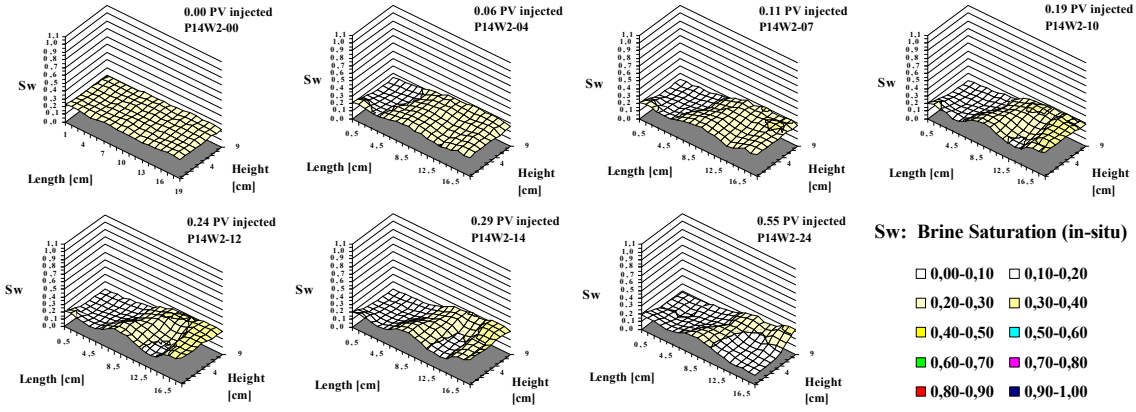

Fig.6 Saturation development of the in-situ water while waterflooding fractured block CHP-12.

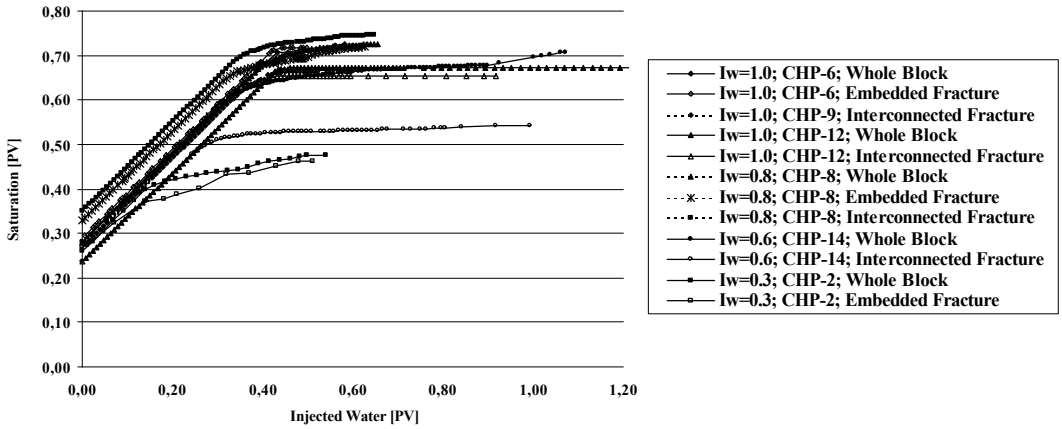

Fig.7 Water saturation when waterflooding whole and fractured block CHP-2 (ref.4), CHP-6 (ref.4), CHP-8, CHP-9, CHP-12 and CHP-14.

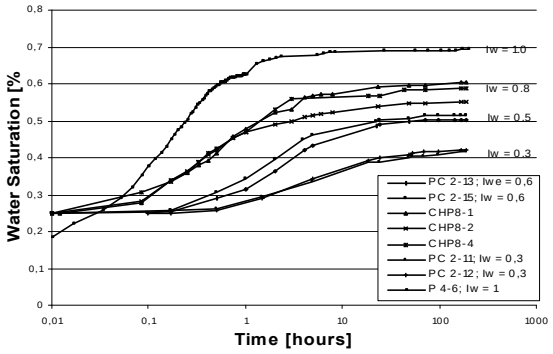

Fig.8 a) Imbibition characteristics for the duplicate core plugs and drilled-out plugs, from the moderately water-wet block CHP-8.

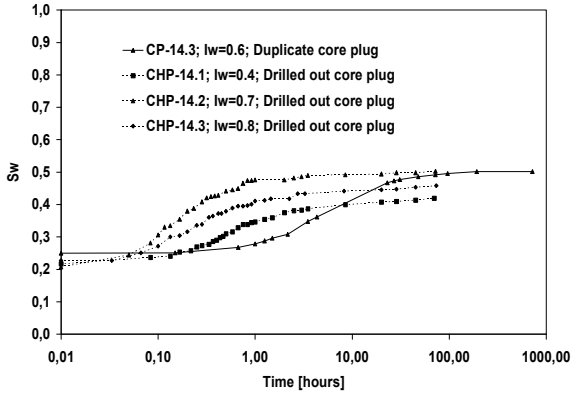

Fig.8 b) Imbibition characteristics for the duplicate core plug and drilled-out plugs, from the moderately water-wet block CHP-14.

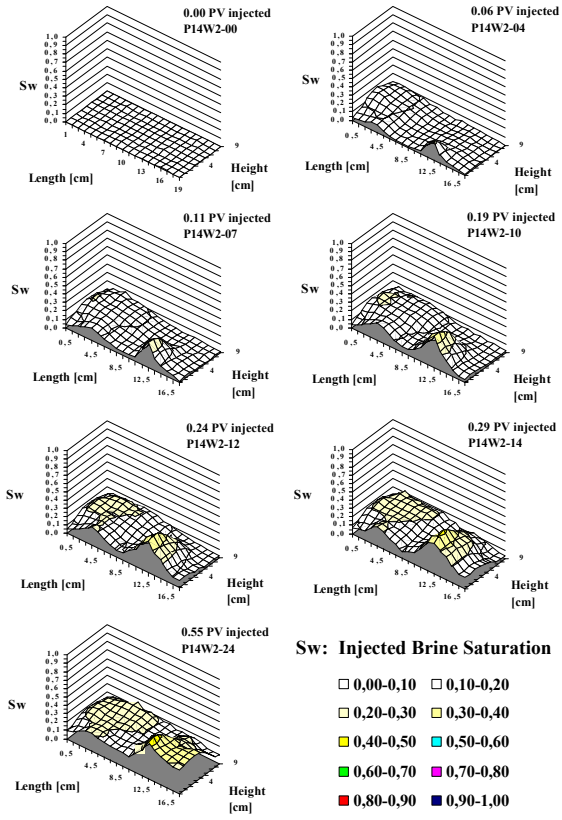

Fig.9 Saturation development of the injected water while waterflooding fractured block CHP-14.

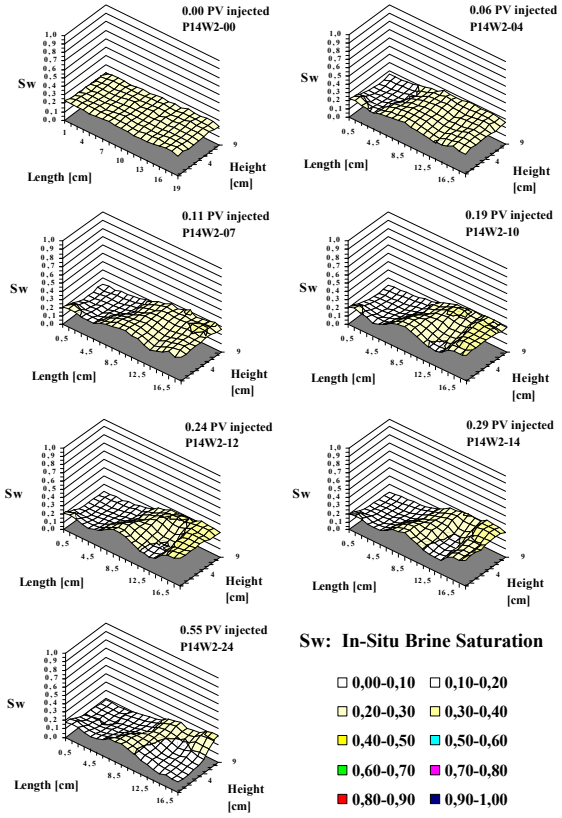

Fig.10 Saturation development of the in-situ water while waterflooding fractured block CHP-14.

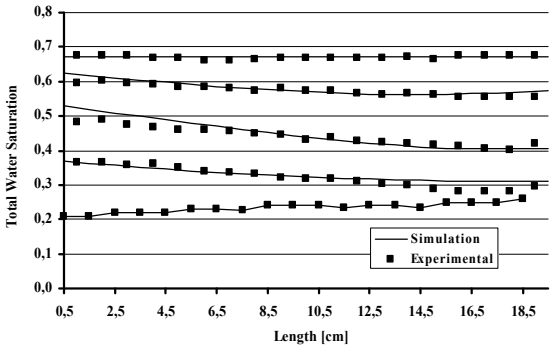

Fig.11 Comparison of experimental and simulated water profiles averaged over cross section of block, when waterflooding whole block CHP-12.

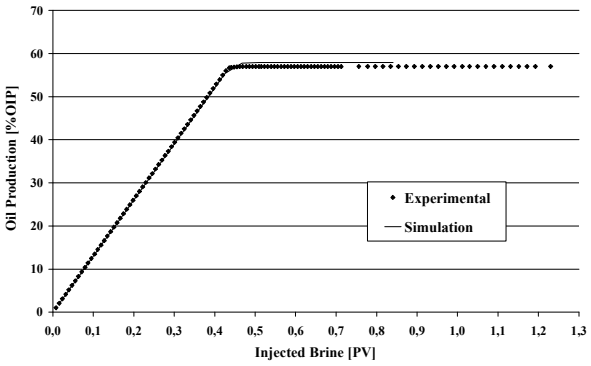

Fig.12 Experimental and simulated oil production when waterflooding whole block CHP-12.

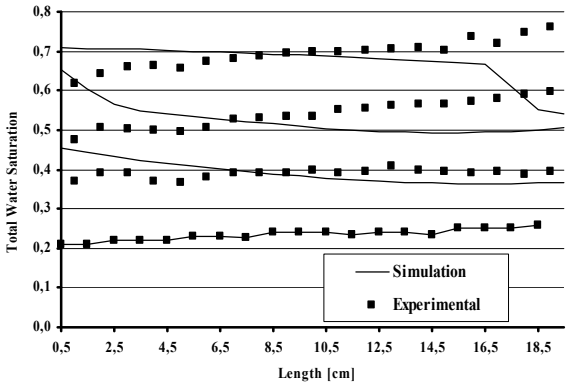

Fig.13 Experimental and simulated water profiles averaged over cross section of block, when waterflooding whole block CHP-14, using homogeneous wettability conditions in the simulation.

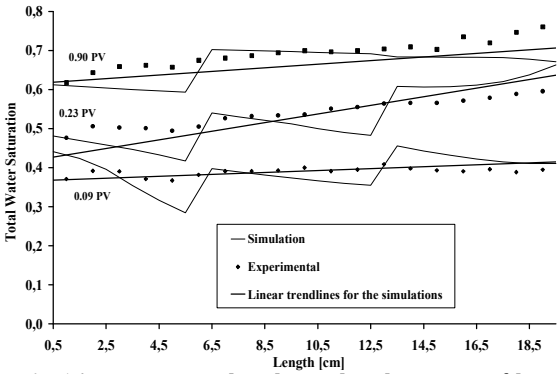

Fig.14 Experimental and simulated water profiles averaged over cross section of block, when waterflooding whole block CHP-14, using heterogeneous wettability conditions in the simulation.